J Mater Sci (2013) 48:4128–4136
DOI 10.1007/s10853-013-7225-9

Sintering and devitrification of glass-powder compacts in the akermanite–gehlenite system

Allu Amarnath Reddy · Dilshat U. Tulyaganov · Ashutosh Goel · Saurabh Kapoor · Maria J. Pascual · José M. F. Ferreira

Received: 22 August 2012 / Accepted: 6 February 2013 / Published online: 13 February 2013

Abstract The sintering and devitrification behavior of glass-powder compacts with four compositions, $Ca_2Mg_{0.5}Al_{1.0}Si_{1.5}O_7$, $Ca_2Mg_{0.6}Al_{0.8}Si_{1.6}O_7$, $Ca_2Mg_{0.7}Al_{0.6}Si_{1.7}O_7$, and $Ca_2Mg_{0.8}Al_{0.4}Si_{1.8}O_7$, corresponding to akermanite–gehlenite ratios (mol%) of 50/50, 60/40, 70/30, and 80/20 were investigated. Glass frits were prepared by the classical melt quenching technique in water. The structure of the glasses was investigated using FTIR and NMR, whereas the sintering behavior was studied by DTA and HSM. Sintering precedes crystallization only in $Ca_2Mg_{0.5}Al_{1.0}Si_{1.5}O_7$ glass while in the remaining glass compositions maximum densification was achieved slight after the onset of crystallization. However, the ratios of final area/initial area (A/A_0) of the glass-powder compact ranging from 0.63 to 0.66 imply towards good densification levels (95–98 %) achieved in the investigated glasses. Qualitative and quantitative XRD analyzes were performed in glass-powder compacts heat treated at 900 and 1000 °C. Merwinite was found to crystallize first followed by decomposition at higher temperatures to form akermanite-like phase.

A. A. Reddy · D. U. Tulyaganov · S. Kapoor · J. M. F. Ferreira (✉)
Department of Materials and Ceramics Engineering, CICECO, University of Aveiro, 3810-193 Aveiro, Portugal
e-mail: jmf@ua.pt

D. U. Tulyaganov
Turin Polytechnic University in Tashkent, 100095 Tashkent, Uzbekistan

A. Goel
Sterlite Technologies Ltd., E-1, E-2, E-3, MIDC, Waluj, Aurangabad 431136, Maharashtra, India

M. J. Pascual
Instituto de Cerámica y Vidrio (CSIC), Kelsen 5, Campus de Cantoblanco, 28049 Madrid, Spain

Introduction

The melilites belong to the family of sorosilicates with general formula $(Ca, Na)_2(Al, Mg, Fe^{2+})[(Al, Si)SiO_7]$ and exist in igneous, as well as metamorphic rocks [1]. Most naturally occurring melilite minerals are solid solutions (ss) of akermanite $[Ca_2(MgSi_2O_7)]$, gehlenite $[Ca_2(Al_2SiO_7)]$, Fe-akermanite $[Ca_2(Fe^{2+}Si_2O_7)]$, and Na-melilite $[NaCa(AlSi_2O_7)]$ [2]. These minerals crystallize from calcium-rich, alkaline magmas and form many artificial melts and blast-furnace slags [3]. Although melilites close in composition to these ideal end members are rare in nature, all the end members (akermanite [4], gehlenite [5], Fe-akermanite [6], and Na-melilite [7]) have been synthetically synthesized [8].

The pioneering study towards understanding the temperature–compositional relationships in this binary system was made by Ferguson and Buddington in 1920, and it was reported that the eutectic composition in this system corresponds 28 wt% gehlenite and 72 wt% akermanite with its melting temperature at 1385 °C [9]. Further, Warren [10] and Smith [11] elucidated the atomic and molecular structure of minerals in this binary system, which was further incremented by studies of Kimata and Ii [12] and Swainson et al. [13]. In a recent study by Merlini et al. [14], in situ X-ray diffraction (XRD) has been employed to study the influence of gehlenite/akermanite ratio on the structure of melilite minerals at high temperature. It has been reported that volumetric thermal expansion increases with decreasing gehlenite/akermanite ratio in minerals and has been shown to depend on the cation content in the tetrahedral T1 site of the structure.

According to the best of our knowledge, no studies on sintering glass-powder compacts in the pure akermanite–gehlenite system were conducted. Only the devitrification of bulk glasses, has been already reported [15, 16]. Orsini et al. [15] demonstrated that glasses along akermanite–gehlenite join with compositions $2CaO{\cdot}(1-x)MgO{\cdot}xAl_2O_3{\cdot}(2-x)SiO_2$, devitrify directly into a product having the same composition for $x > 0.6$, while glasses with $x < 0.6$ tend to devitrify into a product having the initial glass composition but via the formation of merwinite $[Ca_3Mg(SiO_4)_2]$ as an intermediate crystalline phase. Also, Małecki et al. [17, 18] studied the influence of Nd (2 mol%) on devitrification kinetics of bulk glasses along gehlenite–akermanite join using differential thermal analysis (DTA) and spectroscopic techniques. The devitrification kinetics were independent of the presence of Nd and the values of activation energy of crystallization were of the same order of magnitude as that for viscous flow in molten silicates (ca. 650–750 kJ mol^{-1}).

This study aims at investigating the sintering ability of fine glass-powder compacts in the akermanite–gehlenite system, which is of high technological relevance for developing advanced glass–ceramic materials, and also at getting deeper insight on the crystallization mechanism when starting from glass-powder frits. As it has been shown in our previous study [19], proper sintering ability is crucial for sealing ceramic and metallic surfaces of SOFCs components by glass that is applied in the powder/slurry form on the ceramic or metallic surfaces to seal the joints.

Experimental

Synthesis of glasses

Four glasses with nominal compositions corresponding to gehlenite/akermanite ratio (mol%):50/50 ($Ca_2Mg_{0.5}Al_{1.0}Si_{1.5}O_7$), 40/60 ($Ca_2Mg_{0.6}Al_{0.8}Si_{1.6}O_7$), 30/70 ($Ca_2Mg_{0.7}Al_{0.6}Si_{1.7}O_7$), and 20/80 ($Ca_2Mg_{0.8}Al_{0.4}Si_{1.8}O_7$) were synthesized by melt-quench technique. Table 1 presents the detailed compositions of the glasses. The glasses have been labeled in accordance with their respective akermanite content (mol%), i.e., Ak-50, Ak-60, Ak-70, and Ak-80.

Powders of technical grade SiO_2 (purity > 99.5 %) and $CaCO_3$ (>99.5 %), and of reactive grade $MgCO_3$ and Al_2O_3 were used. Homogeneous mixture of batches (~100 g), as given in Table 1, obtained by ball milling, was preheated at 900 °C for 1 h for decarbonization and then melted in Pt–Rh crucibles at 1590 °C for 1 h, in air. Glasses in frit form were produced by quenching of glass melts in cold water. The frits were dried and then milled in a high-speed agate mill resulting in fine glass powders with mean particle sizes of 15–20 μm (determined by light scattering technique; Coulter LS 230, Beckman Coulter, Fullerton, CA; Fraunhofer optical model). The amorphous nature of glasses was confirmed by XRD analysis (Rigaku Geigerflex D/Max, Tokyo, Japan; C Series; Cu Kα radiation; 2θ range 10°–80°; step 0.02° s^{-1}).

Table 1 Batch compositions of the glasses

Glass	CaO	MgO	Al_2O_3	SiO_2
Ak-50				
Wt%	41.02	7.37	18.64	32.96
Mol%	44.45	11.11	11.11	33.33
Molar ratio	1.00	0.25	0.25	0.75
Ak-60				
Wt%	41.05	8.85	14.92	35.18
Mol%	43.48	13.04	8.69	34.78
Molar ratio	1.00	0.30	0.20	0.80
Ak-70				
Wt%	41.07	10.33	11.20	37.40
Mol%	42.56	14.89	6.38	36.17
Molar ratio	1.00	0.35	0.15	0.85
Ak-80				
Wt%	41.09	11.81	7.47	39.62
Mol%	41.67	16.66	4.17	37.50
Molar ratio	1.00	0.40	0.10	0.90

Structural characterization of glasses

Infrared spectra for the glass powders were obtained using an infrared Fourier spectrometer (FTIR, model Mattson Galaxy S7000, USA). For this purpose, each sample powder was mixed with KBr in the proportion of 1/150 (by weight) and pressed into a pellet using a hand press. 64 scans for background and 64 scans per sample were made with signal gain 1. The resolution was 4 cm^{-1}.

^{29}Si magic angle spinning (MAS) nuclear magnetic resonance (NMR) spectra were recorded on a Bruker ASX 400 spectrometer operating at 79.52 MHz (9.4 T) using a 7-mm probe at a spinning rate of 5 kHz. The pulse length was 2 μs and 60 s delay time was used. Kaolinite was used as the chemical shift reference. ^{27}Al MAS-NMR spectra were recorded on a Bruker ASX 400 spectrometer operating at 104.28 MHz (9.4 T) using a 4-mm probe at a spinning rate of 15 kHz. The pulse length was 0.6 μs and 4 s delay time was used. $Al(NO_3)_3$ was used as the chemical shift reference.

Thermal analysis of glasses

A side-view hot-stage microscope (HSM) EM 201 equipped with image analysis system and electrical furnace 1750/15 Leica was used. The microscope projects the image of the sample through a quartz window and onto the

recording device. The computerized image analysis system automatically records and analyzes the geometry changes of the sample during heating. The image analyzer takes into account the thermal expansion of the alumina substrate while measuring the height of the sample during firing, with the base as a reference. The HSM software calculates the percentage of decrease in height, width, and area of the sample images. The measurements were conducted in air with a heating rate (β) of 5 K min^{-1}. The cylindrical-shaped samples with height and diameter of $\approx$3 mm were prepared by cold-pressing the glass powders. The cylindrical samples were placed on a 10 × 15 × 1 mm alumina (>99.5 wt% Al_2O_3) support. The temperature was measured with a Pt/Rh (6/30) thermocouple contacted under the alumina support. The temperatures corresponding to the characteristic viscosity points (first shrinkage, maximum shrinkage, softening, half ball, and flow) were obtained from the photographs taken during the hot-stage microscopy experiment following Scholze's definition [20, 21].

DTA of fine powders was carried out in air (DTA–TG, Labsys Setaram, Setaram Instrumentation, Caluire, France). DTA scans were recorded from room temperature to 1000 °C at a heating rate of 5 K min^{-1}. The values of the glass transition temperature (T_g), crystallization onset temperature (T_c), and peak temperature of crystallization (T_p) were obtained from the DTA thermographs of the respective glasses.

Crystalline phase evolution in glass–ceramics

Circular disk-shaped pellets with 20 mm diameter and thickness ~3 mm were prepared from glass powders by uniaxial pressing (80 MPa). The samples were sintered under non-isothermal conditions for 1 h at 900 and 1000 °C, respectively. A slow heating rate of 2 K min^{-1} was maintained in order to prevent deformation of the samples. Qualitative as well as quantitative phase analysis of glass–ceramics (crushed to particle size <63 μm) was made by XRD using a conventional Bragg–Brentano diffractometer (Philips PW 3710, Eindhoven, The Netherlands) with Ni-filtered Cu Kα radiation in conjunction with combined Rietveld–RIR method. The 10 wt% of corundum (NIST SRM 674a, annealed at 1500 °C for 1 day to increase the crystallinity to 100 %) was added to all the glass–ceramics samples as an internal standard. The mixtures, ground in an agate mortar, were side loaded in aluminum flat holder in order to minimize the preferred orientation problems. Data were recorded in 2θ-range of 5°–120° (step size 0.02° and 6 s of counting time for each step). The phase fractions were extracted by Rietveld–RIR refinements, using GSAS software and EXPGUI as graphical interface, were rescaled on the basis of the absolute weight of corundum originally added to their mixtures as an internal standard, and therefore, internally renormalized. The background was successfully fitted with a Chebyshev function with a variable number of coefficients depending on its complexity. The peak profiles were modeled using a pseudo-Voigt function with one Gaussian and one Lorentzian coefficient. Lattice constants, phase fractions, and coefficients corresponding to sample displacement and asymmetry were also refined.

Electrical conductivity of glass–ceramics

The total conductivity was studied by the AC impedance spectroscopy (Potentistat/Galvanostat/ZRA, Reference 600, 10 Hze1 MHz; Gamry Instruments, Warminster, PA, USA) using dense disk-shaped samples (sintered at 900 °C for 1 h) with porous Pt electrodes and Pt current collectors, in atmospheric air. In the course of impedance measurements, the magnitude of AC voltage was fixed at 1.00 V. The electrical conductivity experiments were performed on a minimum of three samples for each composition in order to confirm the accuracy of the measurements.

Thermal expansion behavior of glass–ceramics

Dilatometry measurements were done on prismatic glass–ceramic samples with a cross section of 4 mm × 5 mm (Bahr Thermo Analyze DIL801 L, Hüllhorst, Germany; heating rate 5 K min^{-1}). The dilatometry measurements were made on a minimum of three samples from each composition and the standard deviation for the reported values of coefficient of thermal expansion (CTE) are in the range of $\pm 0.1 \times 10^{-6}$ K^{-1}.

Results

The proneness of the experimental glasses to an easy devitrification due to high crystal growth rate [15] hindered obtaining true glasses in bulk form. Therefore, glass melts after holding at 1590 °C for 1 h were quickly poured into cold water to produce transparent glass frits of amorphous nature as confirmed by XRD analysis (not shown). The room temperature FTIR transmittance spectra of the investigated glasses are shown in Fig. 1. The most intense broad band in the 800–1200 cm^{-1} region indicates the distribution of stretching vibrations of the SiO_4 tetrahedron with different numbers of bridging oxygen atoms with the center of gravity fixed at ~950 cm^{-1} (small chain Q^2 units) while the band in the 300–600 cm^{-1} region corresponds to bending vibrations of Si–O–Si and Si–O–Al linkages. With respect to the aluminum coordination in glass structure, the presence of transmittance band from medium to strong intensity in the 650–750 cm^{-1} region with the center of gravity at ~700 cm^{-1} is a typical feature of per-alkaline glasses and

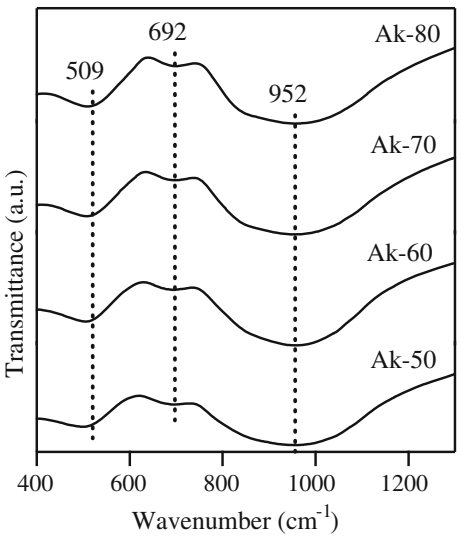

Fig. 1 FTIR spectra of the investigated glass powders

implies towards the tetrahedral coordination of Al [22, 23]. Further, although an increase in akermanite content in glasses did not affect the major silicate band in the region 800–1200 cm^{-1}, slight shoulder formation was observed at ~845 cm^{-1} possibly due to the presence of Q^0 (Si) structural units [24]. These observations can be attributed to the modifying effect of increasing contents of alkaline-earth oxides and the concomitant decreasing amount of network forming Al_2O_3 in glasses [23].

Figure 2 presents the MAS-NMR spectra of the investigated glasses for ^{29}Si (Fig. 2a) and ^{27}Al (Fig. 2b) nuclei. The broad ^{29}Si spectra of all the glasses imply towards a wider distribution of Q^n (Si) units in their structure. At the same time, no significant variations in the peak positions of ^{29}Si and ^{27}Al spectra could be observed indicating the minimal effect of varying akermanite/gehlenite ratio on the silicon and aluminum environment. With respect to silicon coordination in glasses, the predominant feature which determines to a first approximation the isotropic ^{29}Si chemical shifts is the number of Si and Al atoms attached to the SiO_4 unit being considered in solid aluminosilicates with increasing polymerization of Q^n building units, i.e., the shielding of central Si atom increases in the sequence $Q^0 < Q^1 < Q^2 < Q^3 < Q^4$ [25]. According to Murdoch et al. [26] an increase in the number of Al next-nearest neighbors deshields the Si nucleus, on average, by 5.5 ppm/Al neighbor. The $^{[4]}Al$ resonance bands in all the glasses exhibit typical asymmetric forms with tails extending towards lower frequency resulting from the distributions in quadrupolar coupling constants.

DTA and HSM curves along with variation in the relative area and heat flow with respect to temperature are presented in Fig. 3. The DTA thermograph of glass Ak-50 presents some apparent overlapped exothermic effects with a weak first peak temperature of crystallization (T_{p1}) at ~900 °C followed by a broad but intense crystallization peak (T_{p2}) at ~940 °C. The intensity of first crystallization peak (T_{p1}) increased with increasing akermanite contents, while the temperature at which it occurs shifted to lower values for glasses Ak-70 and Ak-80. Oppositely, the crystallization peak (T_{p2}) tended to appear at slightly higher temperatures with increasing akermanite contents (except Ak-80 glass), thus resulting in two distinct and well-defined crystalline exotherms.

From HSM data, all the glasses demonstrated single-step sintering behavior with their temperatures for first shrinkage (T_{FS}; log $\eta = 9.1 \pm 0.1$, η is viscosity; dPa s) and for

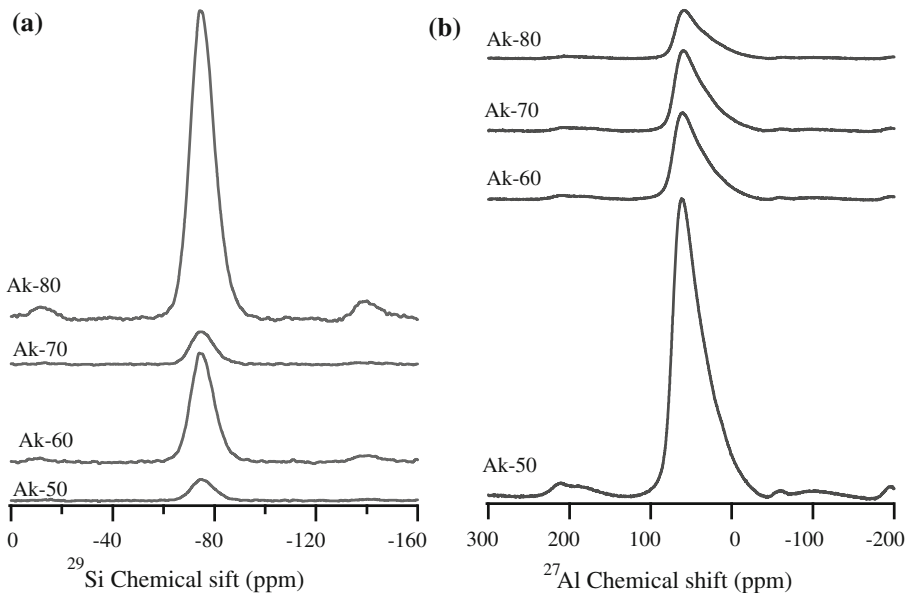

Fig. 2 **a** ^{29}Si MAS-NMR spectra and **b** ^{27}Al MAS-NMR spectra of the investigated glasses

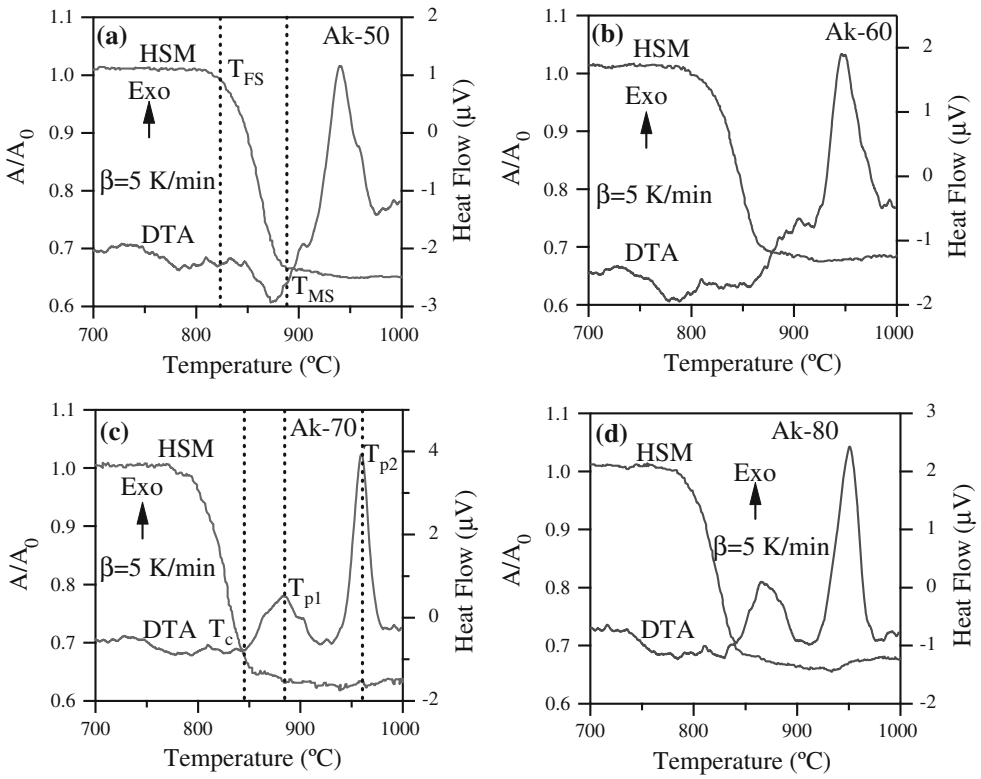

Fig. 3 Comparison of HSM and DTA curves on the same temperature scale for glass compositions: **a** Ak-50, **b** Ak-60, **c** Ak-70, and **d** Ak-80

maximum shrinkage (T_{MS}; log $\eta = 7.8 \pm 0.1$) decreasing with increasing akermanite contents as is evident from Fig. 3. Maximum densification (T_{MS}) was achieved slight before the onset of crystallization (T_c) in Ak-50 glass, whereas in the remaining investigated glasses maximum densification was achieved slight after the onset of crystallization. Characteristic parameters obtained from DTA and HSM curves are summarized in Table 2. The photomicrographs of the glass powders do not exhibited any considerable change in the dimensions of the samples until 1300 °C (Fig. 4), however, the ratios of final area/initial area (A/A_0) of the glass-powder compact at T_{MS} ranging from 0.62 to 0.66 (Table 2) imply towards good densification levels (95–98 %) achieved in the investigated glasses. Lara et al. [27] proposed a thermal parameter, S_c ($=T_c - T_{MS}$), to estimate the competition between sintering and crystallization of glass powders during heating. The lower value of S_c implies a higher tendency towards glass devitrification. Additionally, the difference between T_c and T_g is often taken as an alternative thermal parameter related to the sintering behavior, with larger differences indicating enhanced sintering ability [28]. Table 2 shows that the interval T_c–T_g decreases from glass Ak-50 to Ak-80 confirming that compositions with lower akermanite contents show smaller tendency to crystallization and greater glass stability. Values obtained for the interval of T_c–T_g are in good correlation with a thermal parameter S_c ($= T_c - T_{MS}$) demonstrating that glass-powder compacts of Ak-50 having a wider range of sintering temperatures in comparison to the other experimental compositions.

Table 2 Influence of glass composition on the thermal parameters obtained from DTA and HSM at $\beta = 5$ K min^{-1}

	Ak-50	Ak-60	Ak-70	Ak-80
$T_g \pm 5$ (°C)	749	746	745	745
$T_{FS} \pm 5$ (°C)	830	805	798	792
$T_{MS} \pm 5$ (°C)	888	880	859	847
$T_c \pm 5$ (°C)	885	860	845	830
$T_d \pm 5$ (°C)	844	1400	1388	1379
$T_{p1} \pm 2$ (°C)	902	906	885	865
$T_{p2} \pm 2$ (°C)	941	949	960	951
$T_{HB} \pm 5$ (°C)	1434	1410	1389	1385
$T_F \pm 5$ (°C)	1445	1417	1391	1388
A/A_0 at T_{MS2}	0.66	0.67	0.63	0.66
S_c ($=T_c - T_{MS}$)	−3	−20	−14	−17
$T_c - T_g$	136	114	100	85

In agreement with HSM and DTA results, well crystalline glass–ceramics were obtained after heat treatment of powder compacts at 900 and 1000 °C for 1 h (Fig. 5). The diffraction peaks corresponding to the crystalline phases appear well defined, suggesting that the crystallization process was already over. Qualitative analysis of X-ray diffractograms of heat-treated samples at 900 °C indicate the akermanite–aluminian ($Ca_2(Al_{0.46}Mg_{0.54})((Al_{0.23}Si_{0.77})_2O_7)$, ICDD:

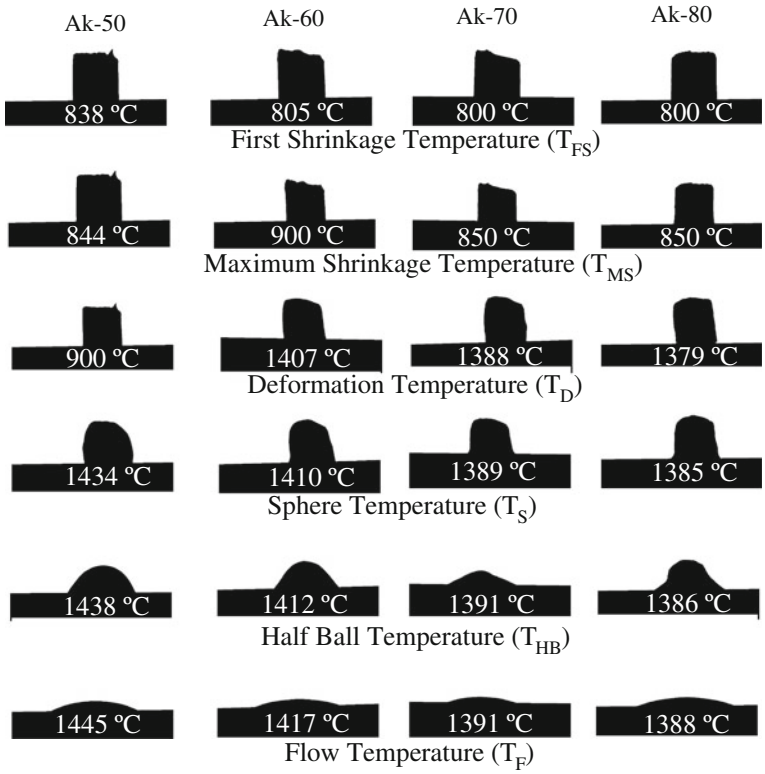

Fig. 4 HSM images of investigated glasses on alumina substrates at various stages of the heating cycle

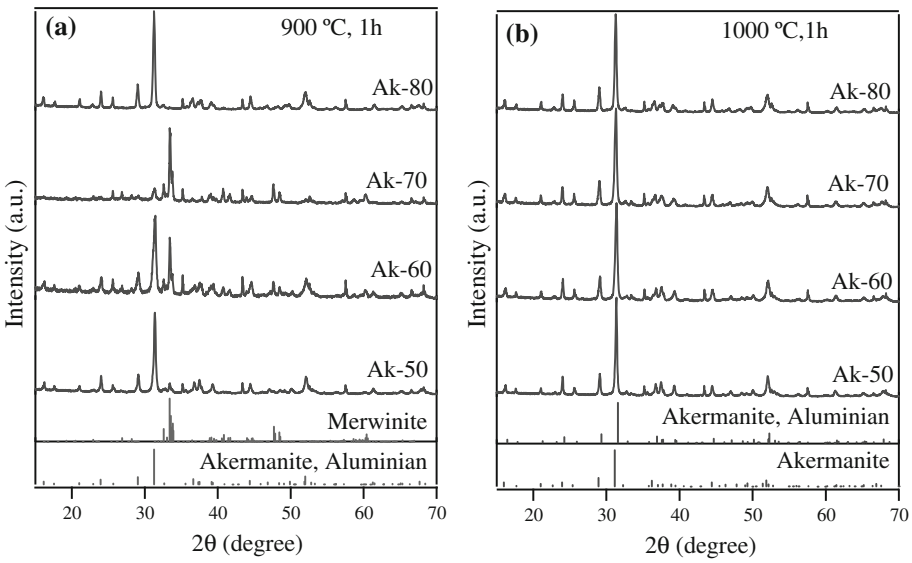

Fig. 5 X-ray diffractograms of glass-powder compacts sintered for 1 h at **a** 900 °C; **b** 1000 °C

076-2633) as the predominant crystalline phase in all the investigated samples, except Ak-70, in which merwinite ($Ca_3Mg(SiO_4)_2$; ICDD: 011-6738) was preferentially formed. At 1000 °C, both akermanite–aluminian ($Ca_2(Al_{0.46}Mg_{0.54})((Al_{0.23}Si_{0.77})_2O_7)$, ICDD: 076-2633) and akermanite (ICDD: 076-0841) appear as the crystalline phases. The quantitative data for crystalline phases as obtained from XRD analysis adjoined with Rietveld–RIR technique are presented in Table 3. Figure 6 shows the fit of a measured XRD pattern of a sintered GC by using the GSAS EXPGUI software. The fitting to the measured X-ray diagram has been performed by a least-square calculation. The calculated diagram (Fig. 6) is based on crystallographic structure models, which also take into account specific instrument and sample effects. The parameters of this model have been refined simultaneously using least-squares methods in order to obtain the best fit to all measured data. By least-squares refinement, a so-called figure-of-merit function *R* has been

Table 3 Rietveld–RIR results showing the dependence of structural features on the composition and heat treatment temperature

	900 °C for 1 h				1000 °C for 1 h			
	Ak-50	Ak-60	Ak-70	Ak-80	Ak-50	Ak-60	Ak-70	Ak-80
Akermanite–Aluminian	77(2)	60(2)	8(1)	58(2)	69(2)	56(2)	44(2)	50(2)
Merwinite	9(1)	24(1)	43(2)	13(1)	–	–	–	–
Akermanite	–	–	–	–	10(1)	23(1)	27(1)	40(2)
Glass	14(2)	16(1)	49(2)	29(1)	11(1)	21(1)	29(1)	10(1)
W_{RP}	0.12	0.15	0.19	0.14	0.11	0.11	0.11	0.12
R_p	0.09	0.11	0.13	0.11	0.08	0.08	0.08	0.09
χ^2	2.52	3.65	5.68	3.39	2.01	2.17	2.11	2.55
R_F^2	0.10	0.18	0.32	0.15	0.06	0.07	0.08	0.09

defined, which describes the residual (agreement) between observed and calculated data [29]. It is noteworthy that many different statistical *R* factors have been proposed for judging the quality of a Rietveld refinement. The *R* factors show the mean deviation in accordance with the model used in percent. The "profile *R*-factor", R_{wp}, for all the refinements are presented in Table 3.

The CTE values of the glass–ceramics measured in the temperature range of 200–700 °C vary in the intervals of (10.16–11.10) and (10.04–10.99) $\times$ 10^{-6} K^{-1}, for the glass–ceramics samples sintered at 900 and at 1000 °C, respectively (Table 4).

The measured electrical conductivity values of the investigated glasses were in the range of 2.3–7.8 $\times$ 10^4 S cm^{-1} at 750 °C, 4.9–15.2 $\times$ 10^4 S cm^{-1} at 800 °C, 8.8–25.5 $\times$ 10^4 S cm^{-1} at 850 °C, and 1.54–5.31 $\times$ 10^5 S cm^{-1} at 900 °C.

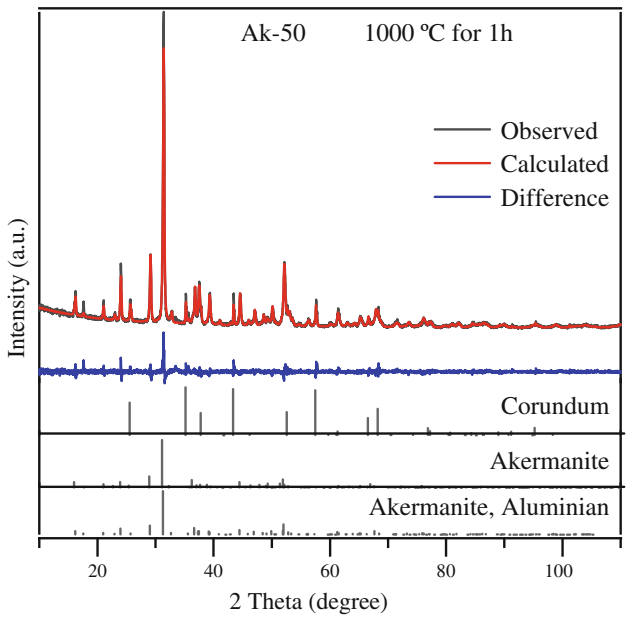

Fig. 6 Observed, calculated, and difference curve from the Rietveld refinement of the Ak-50 glass–ceramics heat treated at 1000 °C for 1 h in air

The activation energy (E_a) for the total conductivity, calculated from the standard Arrhenius equation, $\sigma = \sigma_0/T$. exp $(-E_a)/RT$, where σ_0 is the pre-exponential factor, for all the glass–ceramics studied, varying in the range of ~110–130 kJ mol^{-1} at 750–900 °C (Table 5; Fig. 7).

Discussion

The sintering process plays an important role in determining the properties and applications of advanced glass–ceramics. In general, with respect to sintering and crystallization two different behaviors can be observed for the glasses: (i) T_c appears before maximum density has been reached and the crystallization process starts before complete densification, which tends to hinder further sintering or, (ii) T_c occurs after the final sintering stage, making sintering, and crystallization-independent processes, and the resultant glass–ceramic is well

Table 4 Influence of glass composition and of heat treatment temperature on the CTE $\times$ 10^{-6} (±0.01) K^{-1} (200–700 °C) of the glass–ceramics

	900 °C for 1 h	1000 °C for 1 h
Ak-50	11.10	10.04
Ak-60	10.16	10.59
Ak-70	10.45	10.92
Ak-80	10.48	10.99

Table 5 Influence of glass composition on the electrical properties of glass–ceramics sintered at 900 °C for 1 h

Composition	σ $\times$ 10^5 (S cm^{-1})				E_a (kJ mol^{-1})
	750	800	850	900	
Ak-50	0.78	1.52	2.55	5.31	123.99
Ak-60	0.23	0.49	0.88	1.74	130.61
Ak-70	0.27	0.53	0.96	1.54	120.32
Ak-80	0.54	1.03	1.77	2.70	110.57

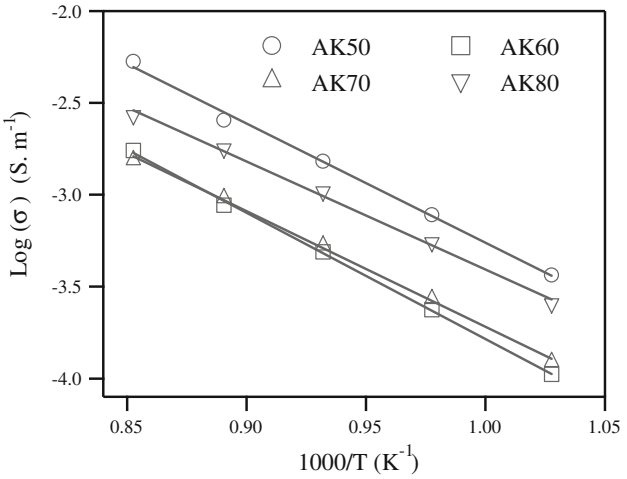

Fig. 7 Arrhenius plot for determination of activation energy for total electrical conductivity of the investigated glass–ceramics

sintered and mechanically strong (a desired trait for a suitable SOFC seal). Oppositely, uncontrolled crystallization during the initial sintering process can lead to the formation of a porous sealing layer that can adversely affect the SOFC operation [19].

Gehlenite is an Al-rich end-member of the melilite and forms complete solid solution series with akermanite with a general formula of $Ca_2Mg_xAl_{2(1-x)}Si_{(1+x)}O_7$. The isomorphous replacements in end members of melilite may occur by the scheme $Mg^{2+} + Si^{4+} \leftrightarrow 2Al^{3+}$ [30] suggesting substitution of aluminum for Mg in the tetrahedral sites MgO_4^{6-} and for Si in the diortogroups $Si_2O_7^{6-}$. Studies on the thermal expansion of melilites from Merlini et al. [14], measured by powder XRD in the temperature range of 25–925 °C concluded that CTE values varied in the range of 10.0–11.0 $\times$ 10^{-6} K^{-1}. It is well known that glass–ceramics having CTE values lower than those of SOFCs components will be under compressive stresses. Accordingly, they will exhibit the ability to resist micro-cracking and retain a hermetic seal.

In this study, glass powder compacts with akermanite fraction lying in the interval 50–80 mol% were investigated. From the NMR spectra of the investigated glasses Ak-50, Ak-60, Ak-70, and Ak-80 (Fig. 2), the ^{29}Si peak position lies at ~ -75 ppm that may represent highly polymerized species with many Al neighbors or less polymerized units with low or no Al neighbors. In the present scenario, the latter option with less polymerized silicate units (a mixture of $Q^1 + Q^2$ units) and low or no Al neighbors seem to be more feasible. This explanation is well supported by the decrease in T_g of glasses with increasing akermanite content as shown in Table 2. Additionally, the glasses with akermanite content $\geq$40 mol% must contain a certain distribution of SiO^{4-} and $Si_2O_7^{6-}$ groups and other structural units (that can be likely $Si_3O_9^{6-}$ rings) whose presence is needed to satisfy the congruence of the system (O/Si = 3.5) [15].

As identified from qualitative and quantitative analysis of crystalline phases in the glass matrix after the heat treatment of glass powder compacts at 900 and 1000 °C for 1 h (Fig. 6; Table 3), the first exothermic peak implies towards a meta stable merwinite ($Ca_3Mg(SiO_4)_2$) crystalline phase which gets converted into a stable akermanite crystalline phase. The low activation energy ($\sim$690 kJ mol^{-1}) of merwinite [17, 18], as compared to akermanite (1001 kJ mol^{-1}) supports the formation of merwinite at lower temperatures. Further, it is worth noting that in glass–ceramics sintered at higher temperature (i.e., 1000 °C) the merwinite phase completely disappeared while both akermanite–aluminian phase and akermanite were present in the final glass–ceramics. Therefore, we propose formation of akermanite phase at 1000 °C to occur as a pseudomorph of mervinite crystals.

Therefore, two types of melilite ss were formed: (a) akermanite–aluminian phase with relatively higher Al_2O_3 content appearing at an earlier stage of crystallization as a result of preferential substitution of aluminum for Si in $Si_2O_7^{6-}$; (b) akermanite phase with lower Al_2O_3 content formed after decomposition of merwinite between 900 and 1000 °C. Relatively high glassy phase content in the GC Ak-70 (Table 3) at both 900 and 1000 °C can be attributed to a low crystal growth rate that is a characteristic feature of all eutectic type compositions.

The decomposition of merwinite seemingly occurred gradually in the temperature interval 900–1000 °C rather than at once and resulted in a slight increase of CTE of glass–ceramics. The CTE values measured for the present glass–ceramics are in good agreement with those required for glass–ceramic sealants used in solid oxide fuel cells (SOFCs) applications [31]. On the other hand, based on the activation energy for conductivity (E_a) values, the composition Ak-50 is the most electrically conductive one, while compositions Ak-60 and Ak-70 exhibit higher electrical resistivity within the entire investigated temperature region.

Conclusions

1. NMR data demonstrated tetrahedral coordination of aluminum in the glass network. According to both FTIR and NMR results, silicon atoms are localized in Q^2 units. The silicon and aluminum environments in the studied glasses were minimally affected by the akermanite/gehlenite ratio.
2. HSM and DTA revealed single-step sintering and two crystallization exotherms. The first exothermic peak is due to the formation of metastable merwinite crystalline

phase while the second one coincides with the formation of melilite ss.

3. Complete merwinite transformation occurs upon heat treating at 1000 °C with the formation of two types of melilite ss: (1) akermanite–aluminian phase with relatively higher Al_2O_3 content that appeared at earlier stage of crystallization as a result of aluminum substitution preferentially for Si in $Si_2O_7^{6-}$; (2) akermanite phase with lower Al_2O_3 content formed after decomposition of merwinite between 900 and 1000 °C.
4. The A/A_0 ratios of the glass-powder compacts ranging from 0.63 to 0.66 imply towards high densification levels (95–98 %).The glass Ak-50 demonstrated smaller tendency towards crystallization, greater glass stability, and better sintering ability in comparison to other investigated glass compositions.
5. The CTE values of the glass–ceramics are in good agreement with those required for glass–ceramic sealants used in SOFCs applications.

Acknowledgements This study was financially supported by the University of Aveiro, CICECO and FCT, Portugal (PTDC/CTM-CER/114209/2009).

References

1. Wood JA (1988) Ann Rev Earth Planet Sci 16:53
2. Deer WA, Howie RA, Zussman J (1963) Rock forming minerals 1: ortho and ring silicates. Longman, London
3. Osborn EF, Schairer JF (1941) Am J Sci 239:75
4. Merlini M, Gemmi M, Artioli G (2006) Z Kristallogr Suppl 23:419
5. Yoder HS (1950) J Geol 58:221
6. Bowen NL, Schairer JF, Posnjak E (1933) Am J Sci 26:193
7. Nurse RW, Midgley HG (1953) J Iron Steel Res Int 174:121
8. Franklin FF, Robert LH, Philip ER (1987) Am Miner 72:137
9. John BF, Buddington AF (1920) Am J Sci 50:131
10. Warren B (1930) Z Kristallogr 74:131
11. Smith JV (1953) Am Miner 38:643
12. Kimata M, Ii N (1981) N Jahrb Mineral Mh 1:1
13. Swainson IP, Martin TD, Wolfgane WS, Andrew P (1992) Phys Chem Miner 19:185
14. Merlini M, Gemini M, Giuseppe C, Gilberto A (2008) Phys Chem Miner 35:147
15. Orsini PG, Buri A, Marotta A (1975) J Am Ceram Soc 58:306
16. Charlu TV, Newton RC, Kleppa OJ (1981) Geochim Cosmochim Acta 45:1609
17. Małecki A, Lejus AM, Viana B, Vivien D, Collongues R (1994) J Non Cryst Solids 170:161
18. Małecki A, Lejus AM, Viana B, Vivien D, Collongues R (1995) J Therm Anal 44:461
19. Goel A, Reddy AA, Pascual MJ, Gremillard L, Malchere A, Ferreira JMF (2012) J Mater Chem 22:10042
20. Pascual MJ, Pascual L, Duran A (2001) Phys Chem Glasses 42:61
21. Pascual DuranA, Prado MO (2005) Phys Chem Glasses 46:512
22. Tarte P (1967) Spectrochim Acta A 23:2127
23. Sharma SK, Yoder HS Jr, Matson DW (1988) Geochim Cosmochim Acta 52:1961
24. Sharma SK, Yoder HS Jr (1979) Carnegie Inst Wash Yearb 78:526
25. Engelhardt G, Michel D (1987) High resolution solid state NMR of silicates and zeolites. Wiley, Chichester
26. Murdoch JB, Stebbins JF, Carmichael ISE, Pines A (1988) Phys Chem Miner 15:370
27. Lara C, Pascual MJ, Duran A (2004) J Non Cryst Solids 348:149
28. Fernandes HR, Tulyaganov DU, Pascual MJ, Kharton VV, Yaremchenko AA, Ferreira JMF (2012) J Eur Ceram Soc 32:2283
29. Young RA (1993) In: Young RA (ed) The Rietveld method. International Union of Crystallography Monographs on Crystallography, vol 5. Oxford University Press, Oxford, p 1
30. Dear PS (1969) Lithos 3:13
31. Donald IW, Mallinson PM, Metcalfe BL, Gerrard LA, Fernie JA (2011) J Mater Sci 46:1975. doi:10.1007/s10853-010-5095-y